AIAA JOURNAL
Vol. 34, No. 10, October 1996

Nonoscillatory Schemes for Kinetic Model Equations for Gases with Internal Energy States

J. Y. Yang*
National Taiwan University, Taipei 10764, Taiwan, Republic of China
and
J. C. Huang† and C. S. Wang‡
Chung Shan Institute of Science and Technology, Lung-Tan, Taiwan, Republic of China

High-order accurate nonoscillatory schemes based on the discrete ordinate method and the characteristic flux difference splitting method are presented for solving the nonlinear Krook-type kinetic model equations for both monatomic gases and gases possessing internal degrees of freedom. The methods are tested for one-dimensional unsteady shock tube flow and for two-dimensional steady rarefied stream past a NACA 0012 airfoil at angles of attack. The computed results are found in good agreement both with theoretical solutions from Euler and Navier–Stokes calculations and with experimental results. Comparisons of results using kinetic models for both monatomic and diatomic gases are included.

I. Introduction

THE transitional flow regime between continuum and free molecular flow regimes has remained one that is difficult to attack either theoretically or experimentally. The capability to accurately predict the rarefied gas flows over the complete spectrum of flow regimes is thus very desirable. It is well known that the use of continuum Navier–Stokes equations is not valid for treating this transitional regime, and the Boltzmann equation based on the kinetic theory of gases needs to be used. Because of the complexity of the nonlinear integral-differential nature of the equation, analytical solutions of the Boltzmann equation are rare and approximate or numerical solutions may be sought. Perhaps the best known and commonly used numerical method for solving the Boltzmann equation is the direct simulation Monte Carlo (DSMC) method of Bird.[1] Applications of the DSMC method to a great variety of rarefied gas flow problems involving complex geometries have been reported.[2]

The difficulties encountered in the solution of the Boltzmann equation are mainly associated with the nonlinear integral nature of the collision term that contains the details of molecular interaction. To circumvent this difficulty, statistical or relaxation models were often proposed as substitutions. The kinetic model equation proposed by Bhatnagar et al.[3] (BGK) provides a more tractable way to solve comparatively complex problems in rarefied gas dynamics. Kinetic models for gases with internal degrees of freedom that preserve the simplicity of the Krook-type model have also been proposed by Morse[4] and by Holway.[5] All of these kinetic model Boltzmann equations bear a resemblance to the original Boltzmann equation concerning the various order of moments. In addition, the transport properties and the continuum Navier–Stokes equations can be obtained from these nonlinear model Boltzmann equations using a Chapman–Enskog procedure.[6] Thus, instead of solving the full Boltzmann equation, one solves the kinetic model equations and hopes to produce a more economic and efficient way for computing rarefied gas flows. The accuracy and applicability of the various kinetic models just mentioned have been tested against experimental data in the contents of rarefied Couette flow,[7] shock wave structures,[8,9] and a high-speed sharp leading-edge problem.[10]

The objective of this study is to present accurate numerical methods for solving the kinetic model equations to treat general rarefied gas flow problems for both monatomic gases and gases with internal degrees of freedom. We shall present details of the numerical methods and compare solutions with different kinetic models for both monatomic and diatomic gases. A study of rarefied gas flow computations using model Boltzmann equations for monatomic gases has been given in Ref. 11, and the detailed formulation for the case of a monatomic gas can be found there. We shall emphasize the use of kinetic models for gases with internal energy states. First, for each quantum state, the discrete ordinate method[12,13] is applied to the distribution function to replace its continuous dependency on the velocity space by a set of distribution functions that are continuous functions in physical space and time but point functions in velocity space. The energy level is treated quantum mechanically and is also discretized using a Gauss–Laguerre quadrature. Then the resulting partial differential equations are of hyperbolic type and are cast into hyperbolic conservation laws form with nonlinear source term. Once this is done, several well-developed characteristics-based high-resolution methods can be employed to solve them. In this work, we extend and apply our previous characteristic flux difference splitting method and its high-order extension[11,14] to solve the aforementioned inhomogeneous hyperbolic system of conservation laws. The high-order methods were constructed out of the total variation diminishing[15] (TVD) and essentially nonoscillatory (ENO) methods originally developed by Harten et al.[16] It is hoped that the present characteristic-based high-resolution schemes may serve as an accurate numerical tool for treating general rarefied gas flows over objects of arbitrary shapes covering the complete spectrum of flow regimes using kinetic model equations.

In Sec. II, the governing kinetic model equations for gases with internal energy states and related formulations are given. In Sec. III, the discretization of the velocity space and internal energy levels using the discrete ordinate method to render the equations to a set of hyperbolic conservation laws with source term is described. In Sec. IV, high-resolution numerical methods based on the characteristic flux difference splitting method are proposed to integrate the nonhomogeneous hyperbolic conservation laws. Both explicit and implicit methods are included. In Sec. V, numerical results for one- and two-dimensional rarefied gas flows are presented to illustrate the use and to test the accuracy of the numerical methods. Some conclusions are given in Sec. VI.

II. Kinetic Model for Gases with Internal Energy States

In this section we describe the Krook-type kinetic models and related formulations relevant to the present solution method to be presented later. We shall adapt the kinetic models for gases whose molecules possess internal degrees of freedom.[4,5] The kinetic models for monatomic gases can be considered as a special

Received Nov. 18, 1994; revision received Dec. 11, 1995; accepted for publication Jan. 27, 1996.

*Professor, Institute of Applied Mechanics. Member AIAA.
†Associate Research Scientist, Aerodynamics Design Laboratory.
‡Deputy Director, Second Division.

case, and further details can be found in Ref. 11. We consider the Morse–Holway kinetic model Boltzmann equations (without external forces) of the form

$$\partial_t f_l + \boldsymbol{v} \cdot \Delta_{\boldsymbol{x}} f_l = \nu_{\mathrm{el}}(F_{tl} - f_l) + \nu_{\mathrm{in}}(F_{il} - f_l) \tag{1}$$

where $f_l(\boldsymbol{x}, \boldsymbol{v}, t, E_l)$ is the velocity distribution function at energy level E_l that depends on space $\boldsymbol{x}$, molecular velocity $\boldsymbol{v}$, and time t; and ν_{el} and ν_{in} are the elastic and inelastic collision frequencies, respectively. In Eq. (1), F_{tl} and F_{il} are appropriate distribution functions, which can be written as

$$F_{tl} = n_l\left(\frac{m}{2\pi k T_t}\right)^{\frac{3}{2}} \exp\left[-\frac{m}{2kT_t}(\boldsymbol{v}-\boldsymbol{u})^2\right] \tag{2a}$$

$$F_{il} = n_{l\mathrm{eq}}\left(\frac{m}{2\pi k T_T}\right)^{\frac{3}{2}} \exp\left[-\frac{m}{2kT_T}(\boldsymbol{v}-\boldsymbol{u})^2\right] \tag{2b}$$

where k is the Boltzmann constant; m is the molecular mass; n_l is gas number density for each quantum state l, where the index l refers to the entire set of quantum number $\{l\} = l_1, l_2, l_3, \ldots$, necessary to specify the internal state of the molecule; T_t is the translation temperature; T_T is the total temperature; $\boldsymbol{u}$ is the flow velocity; and $n_{l\mathrm{eq}}$ is the equilibrium number density. The various macroscopic moments can be calculated in terms of f_l. The elastic and inelastic collision frequencies are given by

$$\nu_{\mathrm{el}} = \frac{nkT_t}{(1+a)\mu} \tag{3a}$$

$$\nu_{\mathrm{in}} = a\nu_{\mathrm{el}} \tag{3b}$$

$$Z_R = \frac{5(1+a)}{3a} \tag{3c}$$

where the rotational relaxation parameter Z_R has to be obtained by experimental means. In the present work, Z_R is taken to be 3.2. The viscosity μ is assumed to have a temperature dependence

$$\mu/\mu_\infty = (T_t/T_\infty)^\chi \tag{4}$$

where χ is tabulated in Ref. 6. The viscosity coefficient μ_∞ is related to reference mean free path λ_∞ by

$$\mu_\infty = \tfrac{5}{16} m n_\infty \lambda_\infty (2\pi R T_\infty)^{\frac{1}{2}} \tag{5}$$

where the subscript ∞ is referred to the reference condition. Combining Eqs. (3–5) gives

$$\nu_{\mathrm{el}} = \frac{16}{5(1+a)} \frac{nkT_t}{\lambda_\infty m n_\infty (2\pi R T_\infty)^{\frac{1}{2}}} \left(\frac{T_t}{T_\infty}\right)^{-\chi} \tag{6}$$

Reduced Distribution Functions

To illustrate the method, we describe the relevant governing equations for two-dimensional problems. First, to reduce the computer storage requirements, the reduced distribution functions[17] are conventionally introduced:

$$g_l(x, y, t, v_x, v_y, E_l) = \int_{-\infty}^{\infty} f_l(x, y, t, \boldsymbol{v}, E_l)\, dv_z \tag{7a}$$

$$h_l(x, y, t, v_x, v_y, E_l) = \int_{-\infty}^{\infty} v_z^2 f_l(x, y, t, \boldsymbol{v}, E_l)\, dv_z \tag{7b}$$

Define the characteristic velocity C_∞ and time t_∞ as

$$C_\infty = \sqrt{2RT_\infty}, \qquad t_\infty = L/C_\infty$$

where L is a characteristic length of the problem.

Introduce the following nondimensional variables:

$$\hat{x} = x/L, \quad \hat{y} = y/L, \quad \hat{t} = t/t_\infty, \quad \hat{v}_i = v_i/C_\infty$$

$$\hat{n} = n/n_\infty, \quad \hat{u}_x = u_x/C_\infty, \quad \hat{u}_y = u_y/C_\infty$$

$$\hat{T} = T/T_\infty, \quad \hat{E}_l = E_l/kT_\infty, \quad \hat{p} = p/\left(\tfrac{1}{2}mn_\infty C_\infty^2\right)$$

$$\hat{\tau}_{xy} = \tau_{xy}/mn_\infty C_\infty^2, \quad \hat{q}_i = q_i/\left(\tfrac{1}{2}mn_\infty C_\infty^3\right)$$

$$\hat{g}_l = g_l/\left(n_\infty/C_\infty^2\right), \quad \hat{h}_l = h/n_\infty$$

$$\hat{G}_{tl} = G_{tl}/\left(n_\infty/C_\infty^2\right), \quad \hat{H}_{tl} = H_{tl}/n_\infty$$

$$\hat{G}_{il} = G_{il}/\left(n_\infty/C_\infty^2\right), \quad \hat{H}_{il} = H_{il}/n_\infty$$

After nondimensionalizing the equations and integrating out the v_z dependence in Eq. (1) using Eq. (7), the single Morse–Holway kinetic model equation in three space dimensions reduces to two simultaneous equations in two space dimensions and can be cast into inhomogeneous conservation law form as follows:

$$\partial_{\hat{t}} \hat{Q}_l + \partial_{\hat{x}} \hat{F}_l^x + \partial_{\hat{y}} \hat{F}_l^y = \hat{S}_l^{\mathrm{el}} + \hat{S}_l^{\mathrm{in}} \tag{8a}$$

where

$$\hat{Q}_l = \begin{bmatrix} \hat{g}_l(\hat{x}, \hat{y}, \hat{t}, \hat{v}_x, \hat{v}_y) \\ \hat{h}_l(\hat{x}, \hat{y}, \hat{t}, \hat{v}_x, \hat{v}_y) \end{bmatrix}, \quad \hat{F}_l^x = \begin{pmatrix} \hat{v}_x \hat{g}_l \\ \hat{v}_x \hat{h}_l \end{pmatrix}, \quad \hat{F}_l^y = \begin{pmatrix} \hat{v}_y \hat{g}_l \\ \hat{v}_y \hat{h}_l \end{pmatrix}$$

$$\hat{S}_l^{\mathrm{el}} = \begin{bmatrix} \hat{\nu}_{\mathrm{el}}(\hat{G}_{tl} - \hat{g}_l) \\ \hat{\nu}_{\mathrm{el}}(\hat{H}_{tl} - \hat{h}_l) \end{bmatrix}, \quad \hat{S}_l^{\mathrm{in}} = \begin{bmatrix} \hat{\nu}_{\mathrm{in}}(\hat{G}_{il} - \hat{g}_l) \\ \hat{\nu}_{\mathrm{in}}(\hat{H}_{il} - \hat{h}_l) \end{bmatrix} \tag{8b}$$

In Eq. (8),

$$\hat{G}_{tl} = (\hat{n}_l/\pi\hat{T}_t)\exp\left\{-(1/\hat{T}_t)\left[(\hat{v}_x - \hat{u}_x)^2 + (\hat{v}_y - \hat{u}_y)^2\right]\right\} \tag{9a}$$

$$\hat{H}_{tl} = \tfrac{1}{2}\hat{T}_t \hat{G}_{tl} \tag{9b}$$

$$\hat{G}_{il} = (\hat{n}_{l\mathrm{eq}}/\pi\hat{T}_T)\exp\left\{-(1/\hat{T}_T)\left[(\hat{v}_x - \hat{u}_x)^2 + (\hat{v}_y - \hat{u}_y)^2\right]\right\} \tag{10a}$$

$$\hat{H}_{il} = \tfrac{1}{2}\hat{T}_T \hat{G}_{il} \tag{10b}$$

and

$$\hat{\nu}_{\mathrm{el}} = \frac{8}{5(1+a)} \frac{\hat{n}\hat{T}^{(1-\chi)}}{\sqrt{\pi}Kn} \tag{11a}$$

$$\hat{\nu}_{\mathrm{in}} = a\hat{\nu}_{\mathrm{el}} \tag{11b}$$

where $Kn = \lambda_\infty/L$ is the Knudsen number and the choice of mean free path and the characteristic length is problem dependent.

Without causing any confusion we shall drop the ^ sign in the following equations. The macroscopic moments in terms of the reduced distribution functions are

$$n_t = \int_{-\infty}^{\infty}\int_{-\infty}^{\infty} g_l\, dv_x\, dv_y \tag{12a}$$

$$n = \sum_l n_l \tag{12b}$$

$$n_{l\mathrm{eq}} = n\left[\frac{\exp(-E_l/T_T)}{\sum_s \exp(-E_s/T_T)}\right] \tag{12c}$$

$$u_\alpha = \frac{1}{n}\sum_l \int_{-\infty}^{\infty}\int_{-\infty}^{\infty} v_\alpha g_l\, dv_x\, dv_y, \qquad (\alpha = x, y) \tag{12d}$$

$$\frac{3}{2}nT_t = \sum_l \left[\int_{-\infty}^{\infty}\int_{-\infty}^{\infty} h_l\, dv_x\, dv_y + \int_{-\infty}^{\infty}\int_{-\infty}^{\infty}\left(v_x^2 + v_y^2\right) g_l\, dv_x\, dv_y\right] - n\left(u_x^2 + u_y^2\right) \tag{12e}$$

$$T_t = \frac{1}{n}\sum_l n_l E_l \tag{12f}$$

$$T_T = \tfrac{3}{5}T_t + \tfrac{2}{5}T_i \tag{12g}$$

$$p = nT_T \tag{12h}$$

$$q_{\alpha t} = \sum_l \left\{ \int_{-\infty}^{\infty}\int_{-\infty}^{\infty} v_\alpha\left[\left(v_x^2+v_y^2\right)g_l + h_l\right] dv_x dv_y - 2u_x\int_{-\infty}^{\infty}\int_{-\infty}^{\infty} v_\alpha v_x g_l\, dv_x\, dv_y - 2u_y\int_{-\infty}^{\infty}\int_{-\infty}^{\infty} v_\alpha v_y g_l\, dv_x dv_y \right\} + u_\alpha\left(u_x^2+u_y^2-\frac{3}{2}nT_t\right) \tag{12i}$$

$$q_{\alpha i} = \sum_l \int_{-\infty}^{\infty}\int_{-\infty}^{\infty} v_\alpha E_l g_l\, dv_x\, dv_y \tag{12j}$$

$$\tau_{\alpha\beta} = -2\sum_l \int_{-\infty}^{\infty}\int_{-\infty}^{\infty} v_\alpha v_\beta g_l\, dv_x\, dv_y + 2nu_\alpha u_\beta + \delta_{\alpha\beta}p \qquad (\alpha, \beta = x, y) \tag{12k}$$

In Eq. (12), q_{xt} and q_{xi} are the heat flux vectors in the x direction as a result of translational and internal temperatures, respectively, $\tau_{\alpha,\beta}$ are the stress tensor, and $\delta_{\alpha\beta}$ denotes the Kronecker delta. The specific heat is assumed to be constant here since the quantum energy levels are assumed to be spaced close together for the temperature range of present interest.

General Curvilinear Coordinates System

In practical problems we encounter arbitrary geometries, and a system of general curvilinear coordinates is commonly introduced. The conservation equations of the two-dimensional rarefied gas dynamics in general coordinates (ξ, η) can then be written in strong conservation law form as

$$\partial_t Q_l + \partial_\xi F_l^\xi + \partial_\eta F_l^\eta = S_l^{\mathrm{cl}} + S_l^{\mathrm{in}} \tag{13a}$$

where

$$Q_l = J^{-1}\begin{pmatrix} g_l \\ h_l \end{pmatrix}, \quad F_l^\xi = J^{-1}\begin{pmatrix} U^\xi g_l \\ U^\xi h_l \end{pmatrix}, \quad F_l^\eta = J^{-1}\begin{pmatrix} V^\eta g_l \\ V^\eta h_l \end{pmatrix} \tag{13b}$$

with

$$U^\xi = \partial_x\xi\, v_x + \partial_y\xi\, v_y, \qquad V^\eta = \partial_x\eta v_x + \partial_y\eta v_y \tag{14}$$

The metric Jacobian is $J = \partial_x\xi\,\partial_y\eta - \partial_y\xi\,\partial_x\eta$ and the metric terms are given by $\partial_x\xi = J\partial_\eta y$, $\partial_x\eta = -J\partial_\xi y$, $\partial_y\xi = -J\partial_\eta x$, $\partial_y\eta = J\partial_\xi x$. The Jacobian coefficient matrices $A^\xi = \partial F^\xi/\partial Q$ and $B^\eta = \partial F^\eta/\partial Q$ of the transformed equations have real eigenvalues

$$\lambda_1^\xi = \lambda_2^\xi = U^\xi, \qquad \lambda_1^\eta = \lambda_2^\eta = V^\eta \tag{15}$$

Note that both A^ξ and B^η are diagonal matrices:

$$A^\xi = \Lambda^\xi = \mathrm{diag}\{\lambda_i^\xi\}, \qquad B^\eta = \Lambda^\eta = \mathrm{diag}\{\lambda_i^\eta\} \tag{16}$$

For later use we define the split normalized Jacobian matrices as follows:

$$\hat{\Lambda}^{\xi\pm} = \mathrm{diag}\left[\frac{1 \pm \mathrm{sgn}(\lambda_i^\xi)}{2}\right], \quad \hat{\Lambda}^{\eta\pm} = \mathrm{diag}\left[\frac{1 \pm \mathrm{sgn}(\lambda_i^\eta)}{2}\right] \tag{17}$$

where $\mathrm{sgn}(\lambda_i)$ denotes the sign of the eigenvalue λ_i.

III. Discrete Ordinate Method

In Eq. (13), each of the reduced distribution functions at each energy level still remains to be a function of five independent variables in the phase space (for the two-dimensional case). The discretization of the velocity space is done using the discrete ordinate method.[12,13] This is the same as that described in Ref. 11 for monatomic gases. For completeness, we briefly give the necessary elements of the method. The discrete ordinate method, which consists of replacing the integration over velocity space of the distribution functions by an appropriate quadrature, requires the values of the distribution function only at certain discrete velocities. Also, the macroscopic moments given by integrals over molecular velocity space can be evaluated by the same quadrature rule, e.g.,

$$\int_0^\infty \exp(-v^2) g_l(v)\, dv \cong \sum_{\sigma=1}^{N} W_\sigma g_l(v_\sigma) \tag{18}$$

where v_σ $(\sigma = 1, \ldots, N)$ are the positive roots of Hermite polynomial of degree N and the various W_σ are the corresponding weights of the Gauss–Hermite quadrature. The quantum energy levels are assumed to be spaced close together, and the discrete rotational energy levels are replaced by an approximate continuous energy space. Then, following Ref. 10, the energy levels are rediscretized according to the Gauss–Laguerre quadrature and the integral in energy space is evaluated using the same quadrature. For example,

$$\theta\sum_l \exp\left(\frac{-E_l}{T_T}\right) \cong \int_0^\infty \exp\left(\frac{-E}{T_T}\right) dE \cong \sum_{\lambda=1}^{M} R_\lambda \exp(E_\lambda)\exp\left(\frac{-E_\lambda}{T_T}\right) \tag{19}$$

where R_λ are the Gauss–Laguerre weighting coefficients corresponding to the E_λ roots of the Laguerre polynomial of degree M. The discrete energy levels denoted as E_λ are fictitious levels that do not correspond one to one with the actual quantum state E_l. Here, we employ approximate energy levels for rotation with equally spaced energy levels and optimize E_λ in such a way that the error in

$$\sum_s \Delta E_s \exp\left(\frac{-E_s}{T_T}\right) = \int_0^\infty \exp\left(-\frac{E}{T_T}\right) dE \tag{20}$$

is a minimum. When the Gauss–Laguerre quadrature is used, it was shown in Ref. 9 that

$$\Delta E_\lambda = R_\lambda \exp(E_\lambda) \tag{21}$$

Finally, we have

$$n_{\lambda\mathrm{eq}} = nR_\lambda \exp\left[E_\lambda\left(1 - T_T^{-1}\right)\right]/T_T \tag{22}$$

Applying the discrete ordinate method to Eq. (13) for the (v_x, v_y) velocity space and the energy space E, one obtains

$$\partial_t Q_{\lambda,\sigma,\delta} + \partial_\xi F^\xi_{\lambda,\sigma,\delta} + \partial_\eta F^\eta_{\lambda,\sigma,\delta} = S^{\mathrm{cl}}_{\lambda,\sigma,\delta} + S^{\mathrm{in}}_{\lambda,\sigma,\delta} \tag{23a}$$

$$Q_{\lambda,\sigma,\delta} = \frac{1}{J}\begin{bmatrix} g_{\lambda,\sigma,\delta}(\xi,\eta,t) \\ h_{\lambda,\sigma,\delta}(\xi,\eta,t) \end{bmatrix}, \quad F^\xi_{\lambda,\sigma,\delta} = \frac{1}{J}\begin{bmatrix} U^\xi_{\sigma,\delta} g_{\lambda,\sigma,\delta} \\ U^\xi_{\sigma,\delta} h_{\lambda,\sigma,\delta} \end{bmatrix}$$

$$F^\eta_{\lambda,\sigma,\delta} = \frac{1}{J}\begin{bmatrix} V^\eta_{\sigma,\delta} g_{\lambda,\sigma,\delta} \\ V^\eta_{\sigma,\delta} h_{\lambda,\sigma,\delta} \end{bmatrix}, \quad S^{\mathrm{cl}}_{\lambda,\sigma,\delta} = \begin{bmatrix} \nu_{\mathrm{cl}}(G_{t\lambda,\sigma,\delta} - g_{\lambda,\sigma,\delta}) \\ \nu_{\mathrm{cl}}(H_{t\lambda,\sigma,\delta} - h_{\lambda,\sigma,\delta}) \end{bmatrix} \tag{23b}$$

$$S^{\mathrm{in}}_{\lambda,\sigma,\delta} = \begin{bmatrix} \nu_{\mathrm{in}}(G_{i\lambda,\sigma,\delta} - g_{\lambda,\sigma,\delta}) \\ \nu_{\mathrm{in}}(H_{i\lambda,\sigma,\delta} - h_{\lambda,\sigma,\delta}) \end{bmatrix}$$

where $g_{\lambda,\sigma,\delta}$, $h_{\lambda,\sigma,\delta}$, $G_{\lambda,\sigma,\delta}$, and $H_{\lambda,\sigma,\delta}$ represent values of g, h, G, and H evaluated at the discrete velocities (v_σ, v_δ) and discrete energy $E_\lambda (\sigma = -N_1, \ldots, -1, 1, \ldots, N_1; \delta = -N_2, \ldots, -1, 1, \ldots, N_2; \lambda = 1, 2, \ldots, M)$. Here N_1, N_2, and M denote the numbers of

discrete quadrature points used in the v_x, v_y, and E spaces, respectively.

Once the set of the discrete distribution functions $g_{\lambda,\sigma,\delta}$ and $h_{\lambda,\sigma,\delta}$ at each energy level and velocity pair are solved, one can obtain all of the moment integrals using Gauss–Hermite quadrature as

$$n_\lambda = \int_{-\infty}^{\infty}\int_{-\infty}^{\infty}\left[g_\lambda(v_x, v_y, x, y, t)e^{v_x^2}e^{v_y^2}\right]e^{-v_x^2}e^{-v_y^2}\,dv_x\,dv_y$$

$$= \sum_{\sigma=-N_1}^{N_1}\sum_{\delta=-N_2}^{N_2} W_\sigma W_\delta\left(g_{\lambda,\sigma,\delta}e^{v_\sigma^2}e^{v_\delta^2}\right) \tag{24a}$$

$$n = \sum_{\lambda=1}^{M} n_\lambda \tag{24b}$$

$$u_x = \frac{1}{n}\sum_{\lambda=1}^{M}\sum_{\sigma=-N_1}^{N_1}\sum_{\delta=-N_2}^{N_2} W_\sigma W_\delta\left(v_\sigma g_{\lambda,\sigma,\delta}e^{v_\sigma^2}e^{v_\delta^2}\right) \tag{24c}$$

$$\frac{3}{2}nT_t = \sum_{\lambda=1}^{M}\sum_{\sigma=-N_1}^{N_1}\sum_{\delta=-N_2}^{N_2} W_\sigma W_\delta\left[h_{\lambda,\sigma,\delta}\right.$$

$$\left.+\left(v_\sigma^2+v_\delta^2\right)g_{\lambda,\sigma,\delta}\right]e^{v_\sigma^2}e^{v_\delta^2} - n\left(u_x^2+u_y^2\right) \tag{24d}$$

$$q_{xt} = \sum_{\lambda=1}^{M}\left\{\sum_{\sigma=-N_1}^{N_1}\sum_{\delta=-N_2}^{N_2} W_\sigma W_\delta v_\sigma\left[h_{\lambda,\sigma,\delta}+\left(v_\sigma^2+v_\delta^2\right)g_{\lambda,\sigma,\delta}\right]\right.$$

$$\times e^{v_\sigma^2}e^{v_\delta^2} - 2u_x\sum_{\sigma=-N_1}^{N_1}\sum_{\delta=-N_2}^{N_2} W_\sigma W_\delta v_\sigma^2 g_{\lambda,\sigma,\delta}e^{v_\sigma^2}e^{v_\delta^2}$$

$$\left.-2u_y\sum_{\sigma=-N_1}^{N_1}\sum_{\delta=-N_2}^{N_2} W_\sigma W_\delta v_\sigma v_\delta g_{\lambda,\sigma,\delta}e^{v_\sigma^2}e^{v_\delta^2}\right\}$$

$$+nu_x\left(u_x^2+u_y^2\right) - \frac{3}{2}nTu_x \tag{24e}$$

$$\tau_{xy} = \sum_{\lambda=1}^{M}\sum_{\sigma=-N_1}^{N_1}\sum_{\delta=-N_2}^{N_2} W_\sigma W_\delta\left(v_\sigma v_\delta g_{\lambda,\sigma,\delta}e^{v_\sigma^2}e^{v_\delta^2}\right) - nu_xu_y \tag{24f}$$

Other macroscopic quantities can be similarly evaluated.

IV. High-Order Nonoscillatory Schemes

In this section we describe the numerical algorithms for solving the set of equations, Eq. (23). Following Refs. 11 and 14, we consider a high-order extension of Eq. (23) as follows:

$$\partial_t Q_{\lambda,\sigma,\delta} + \left(\hat{\Lambda}_{\sigma,\delta}^{\xi+} + \hat{\Lambda}_{\sigma,\delta}^{\xi-}\right)\partial_\xi F_{\lambda,\sigma,\delta}^{\xi M}$$

$$+\left(\hat{\Lambda}_{\sigma,\delta}^{\eta+} + \hat{\Lambda}_{\sigma,\delta}^{\eta-}\right)\partial_\eta F_{\lambda,\sigma,\delta}^{\eta M} = S_{\lambda,\sigma,\delta}^{\mathrm{el}} + S_{\lambda,\sigma,\delta}^{\mathrm{in}} \tag{25}$$

where $\sigma = -N_1, \ldots, -1, 1, \ldots, N_1, \delta = -N_2, \ldots, -1, 1, \ldots, N_2$, and $\lambda = 1, 2, \ldots, M$. The modified fluxes $F_{\lambda,\sigma,\delta}^{\xi M}$ and $F_{\lambda,\sigma,\delta}^{\eta M}$ are at the discrete points and consist of the original fluxes and additional fluxes of higher-order accuracy that have some nonlinear control mechanism built in to avoid oscillatory solutions in high-gradient regions.

Define a uniform computational mesh system (ξ_j, η_k) with mesh sizes $\Delta\xi = \Delta\eta = 1$ and let $Q_{j,k,\lambda,\sigma,\delta}^n$ denote the value of Q at time level $n\Delta t$, position $(j\Delta\xi, k\Delta\eta)$, discrete velocity point (v_σ, v_δ), and energy level E_λ. Define the difference of the characteristic variables in the local ξ direction as $\alpha_{j+1/2,k,\lambda,\sigma,\delta}^{\xi} = (Q_{j+1,k,\lambda,\sigma,\delta} - Q_{j,k,\lambda,\sigma,\delta})J_{j+1/2,k}$, where $J_{j+1/2,k} = (J_{j,k} + J_{j+1,k})/2$.

Explicit Methods

In terms of operator form, we have the time integration scheme for Eq. (25) as

$$Q_{\lambda,\sigma,\delta}(t+2\Delta t) = \mathcal{L}_x(\Delta t)\mathcal{L}_\xi(\Delta t)\mathcal{L}_\eta(\Delta t)$$

$$\times\,\mathcal{L}_\eta(\Delta t)\mathcal{L}_\xi(\Delta t)\mathcal{L}_x(\Delta t)Q_{\lambda,\sigma,\delta}(t) \tag{26}$$

where the time step Δt is chosen to be less than the local mean collision time τ and satisfy the Courant–Friedrichs–Lewy (CFL) stability condition. The elastic collision time is less than the inelastic collision time, and both must be chosen phenomenologically. The time integration of the governing equations is carried out on each pair of discrete velocity points (v_σ, v_δ) and each energy level E_λ with finite difference approximations. Without causing any ambiguity, we omit the subscripts $(\lambda, \sigma, \delta)$ in the operators $\mathcal{L}_x$, $\mathcal{L}_\xi$, and $\mathcal{L}_\eta$.

The integration of the source term is done using a second-order Runge–Kutta method:

$$Q_{j,k}^* = \mathcal{L}_s(\Delta t)Q_{j,k}^n = Q_{j,k}^n + \Delta t\left(S_{j,k}^{\mathrm{eln}} + S_{j,k}^{\mathrm{inn}}\right) \tag{27a}$$

$$Q_{j,k}^{n+1} = Q_{j,k}^n + \tfrac{1}{2}\Delta t\left(\mathcal{L}_s Q_{j,k}^n + \mathcal{L}_s Q_{j,k}^*\right) \tag{27b}$$

The one-dimensional space operator $\mathcal{L}_\xi(\Delta t)$ is defined by

$$Q_{j,k}^{n+1} = \mathcal{L}_\xi(\Delta t)Q_{j,k}^n = Q_{j,k}^n - \Delta t\left(F_{j+\frac{1}{2},k}^N - F_{j-\frac{1}{2},k}^N\right) \tag{28}$$

with the numerical flux F^N defined by

$$F_{j+\frac{1}{2},k}^N = F_{j+1,k}^{\xi M} - \hat{\Lambda}_{j+\frac{1}{2},k}^{\xi+}\Delta_+ F_{j,k}^{\xi M} = F_{j,k}^{\xi M} + \hat{\Lambda}_{j+\frac{1}{2},k}^{\xi-}\Delta_+ F_{j,k}^{\xi M} \tag{29}$$

where $\Delta_\pm f_j = \pm(f_{j\pm1} - f_j)$ denote the usual forward and backward difference operators. The modified flux $F_{j,k}^{\xi M}$ is expressed as

$$F_{j,k}^{\xi M} = F_{j,k}^{\xi} + E_{j,k}^{\xi} + D_{j,k}^{\xi} \tag{30}$$

To achieve high-order TVD and nonoscillatory schemes,[15,16] one only needs to define E^ξ and D^ξ, and they are given in Refs. 11 and 14.

Implicit Methods

Using the Euler implicit time-differencing formula, Eq. (25) can be written as

$$\left[I + \Delta t(\hat{\Lambda}^{\xi+} + \hat{\Lambda}^{\xi-})\partial_\xi\Lambda^\xi + \Delta t(\hat{\Lambda}^{\eta+} + \hat{\Lambda}^{\eta-})\partial_\eta\Lambda^\eta\right.$$

$$\left.+\,C\right]\Delta Q_{j,k}^{n+1} = \mathrm{RHS}_{j,k}^n \tag{31a}$$

$$\mathrm{RHS}_{j,k}^n = -\Delta t\left[(\hat{\Lambda}^{\xi+} + \hat{\Lambda}^{\xi-})\partial_\xi F^{\xi M}\right.$$

$$\left.+\,(\hat{\Lambda}^{\eta+} + \hat{\Lambda}^{\eta-})\partial_\eta F^{\eta M}\right] + \Delta t S_{j,k}^n \tag{31b}$$

where $\Delta Q^{n+1} = Q^{n+1} - Q^n$, I is the unit matrix, $C = C^{\mathrm{el}} + C^{\mathrm{in}}$, and $C^{\mathrm{el}} = (\partial S^{\mathrm{el}}/\partial Q)$, $C^{\mathrm{in}} = (\partial S^{\mathrm{in}}/\partial Q)$. Equation (31) can be approximately factored in several different ways. We adopt the lower-upper (LU) method,[18] and Eq. (31) becomes

$$[I + \Delta t(L + U + C)]\Delta Q_{j,k}^{n+1} = \mathrm{RHS}_{j,k}^n \tag{32a}$$

where

$$L = \hat{\Lambda}^{\xi+}\delta_\xi^b\Lambda^\xi + \hat{\Lambda}^{\eta+}\delta_\eta^b\Lambda^\eta, \quad U = \hat{\Lambda}^{\xi-}\delta_\xi^f\Lambda^\xi + \hat{\Lambda}^{\eta-}\delta_\eta^f\Lambda^\eta \tag{32b}$$

In Eq. (32), δ^b and δ^f denote the backward and forward difference operators, respectively.

An approximate LU factorization for Eq. (32) can be given as

$$[D + \Delta tL]D^{-1}[D + \Delta tU]\Delta Q_{j,k}^{n+1} = \mathrm{RHS}_{j,k}^n \tag{33a}$$

$$D = I + \Delta tC \tag{33b}$$

It is implemented in the following sequence:

$$[D + \Delta tL]\Delta Q_{j,k}^* = \mathrm{RHS}_{j,k}^n \tag{34a}$$

$$[D + \Delta tU]\Delta Q_{j,k}^{n+1} = D\Delta Q_{j,k}^* \tag{34b}$$

$$Q_{j,k}^{n+1} = Q_{j,k}^n + \Delta Q_{j,k}^{n+1} \tag{34c}$$

The approximation factorization error of Eq. (34) is

$$\mathcal{E}_{LU} = \Delta t^2 LD^{-1}U\Delta Q^{n+1} \tag{35}$$

which can be shown to produce the least amount of error among several possible factorizations, particularly when the norms of the

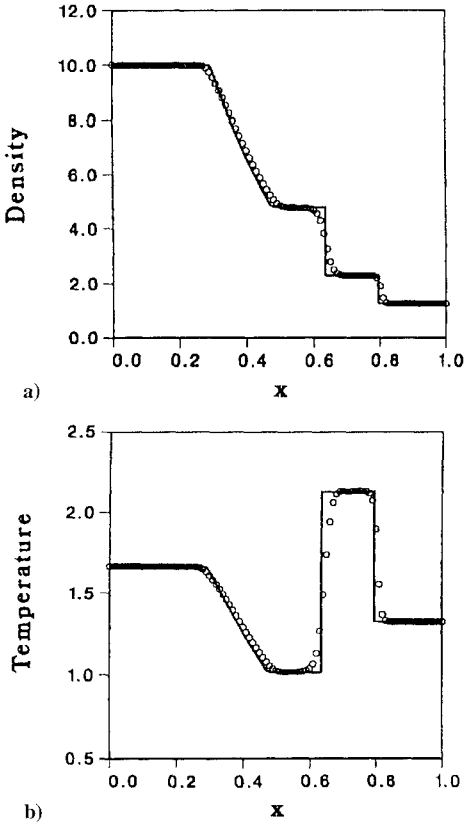

Fig. 1 BGK model (monatomic gas) solution of the shock-tube problem using ENO2 scheme ($\Delta x = 10\lambda_R$): a) density and b) temperature. Symbols denote the computed solution, and solid lines denote the Euler exact solution.

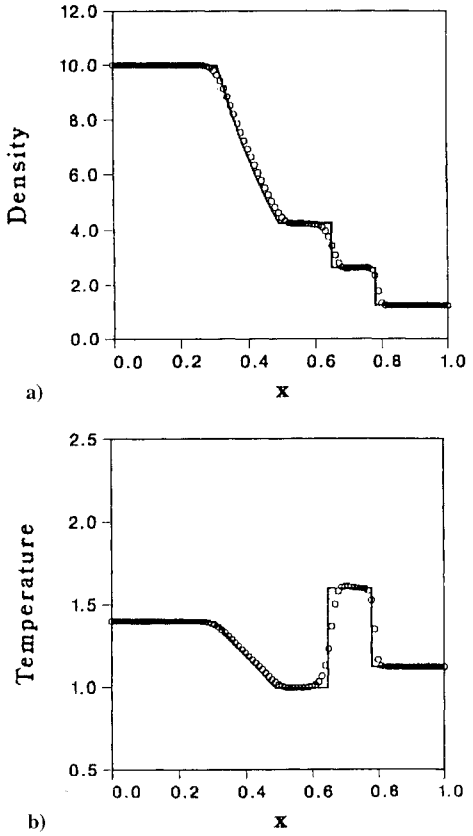

Fig. 2 Morse–Holway model (diatomic gas) solution of the shock-tube problem using ENO2 scheme ($\Delta x = 10\lambda_R$): a) density and b) temperature. Symbols denote the computed solution, and solid lines denote the Euler exact solution.

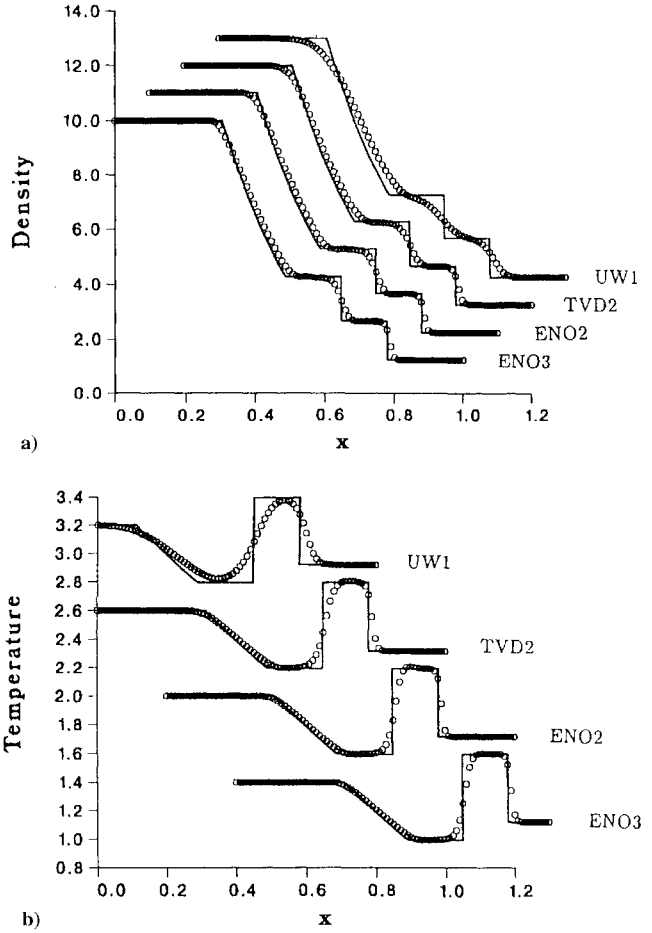

Fig. 3 Morse–Holway model solution of shock-tube problem using various schemes: a) density and b) total temperature.

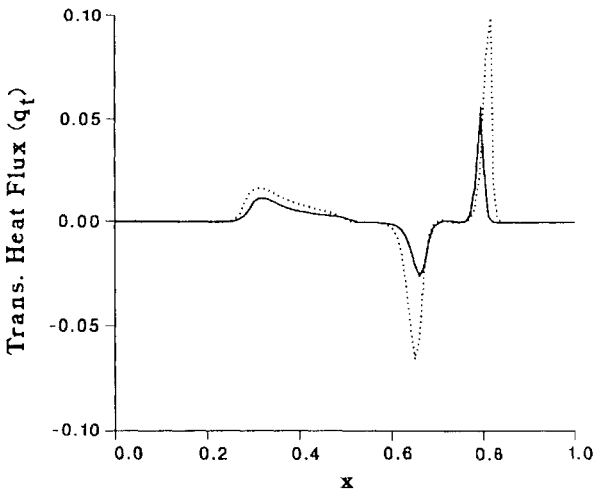

Fig. 4 Translational heat flux distributions along the shock tube using BGK and Morse–Holway kinetic models ($\Delta x = 10\lambda_R$): ——, diatomic gas and · · · · ·, monatomic gas.

source terms are large.[19] The collision source term S of the model equation in general is a functional of the reduced distribution functions $g_{\lambda,\sigma,\delta}$ and $h_{\lambda,\sigma,\delta}$. The exact evaluation of the Jacobian matrix of the source term C is difficult. In this work, we approximate the Jacobian of the source term as

$$C^{\mathrm{el}} \approx \nu_{\mathrm{el}} \begin{pmatrix} -1 & 0 \\ 0 & -1 \end{pmatrix} = \Lambda^{S_{\mathrm{el}}}; \qquad C^{\mathrm{in}} \approx \nu_{\mathrm{in}} \begin{pmatrix} -1 & 0 \\ 0 & -1 \end{pmatrix} = \Lambda^{S_{\mathrm{in}}} \tag{36}$$

With these simplified approximations the equations become diagonal and completely decoupled, and the solution procedure becomes

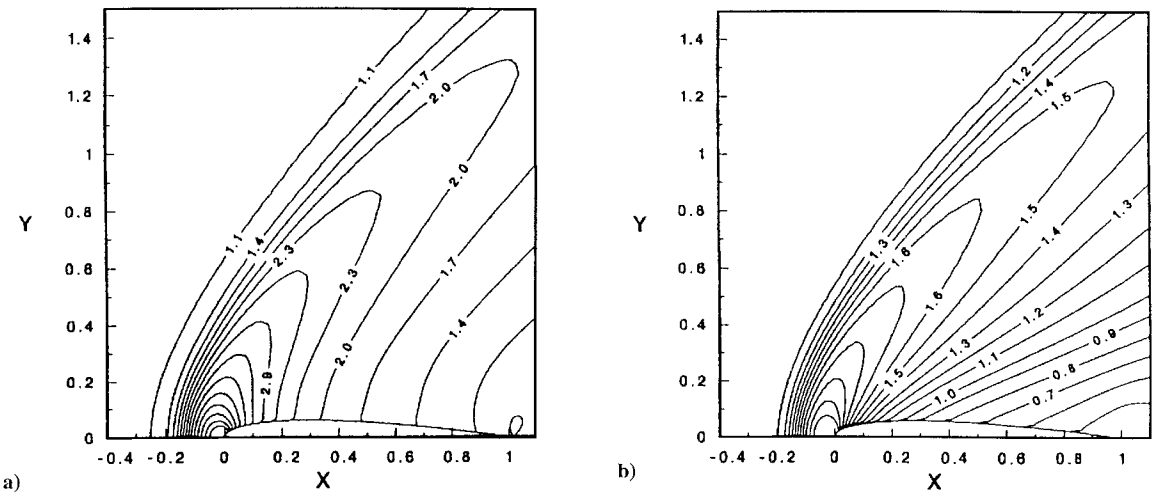

Fig. 5 Supersonic rarefied gas flow past a NACA 0012 airfoil ($M_\infty = 2.0$, $Re_l = 1.06 \times 10^2$, $Kn_\infty = 0.03$, and $\alpha = 0$ deg). BGK model for a monatomic gas: a) pressure contours and b) density contours.

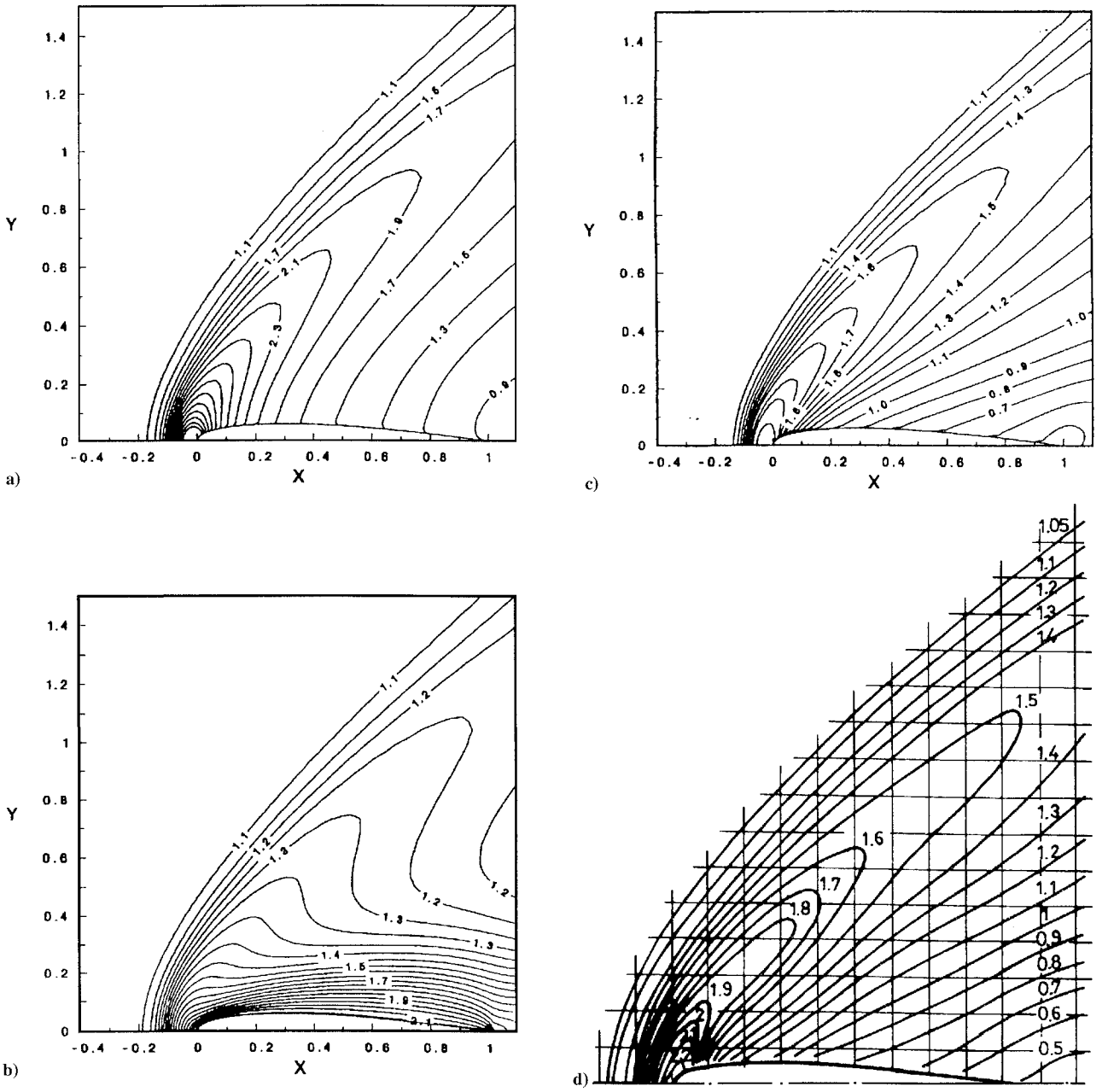

Fig. 6 Supersonic rarefied airflow past a NACA 0012 airfoil ($M_\infty = 2.0$, $Re_l = 1.06 \times 10^2$, $Kn_\infty = 0.03$, and $\alpha = 0$ deg). Morse–Holway model for a diatomic gas: a) pressure contours, b) temperature contours, c) density contours, and d) experiment (ρ/ρ_∞ values).[22]

rather simple and can be solved scalarly. The numerical experience indicates that such an approximation works well.

Boundary Conditions

Initially, the gas is assumed to be in local equilibrium, i.e.,

$$g_l = (n_{leq}/\pi T_T)\exp\{-(1/T_T)[(v_x - u_x)^2 + (v_y - u_y)^2]\} \quad (37a)$$

$$h_l = \tfrac{1}{2} T_{Tgl} \quad (37b)$$

To specify the interaction of the molecules with the solid surface, it is assumed that molecules that strike the surface are subsequently emitted with a Maxwellian velocity distribution characterized by the surface temperature T_w. The two-stream concept is also applied here by defining the half-range distribution functions

$$g_l^+(\xi, \eta; v_x, v_y) = 0, \qquad \text{for} \quad v_n < 0 \quad (38a)$$

$$g_l^-(\xi, \eta; v_x, v_y) = 0, \qquad \text{for} \quad v_n > 0 \quad (38b)$$

where $v_n = \boldsymbol{v}\cdot\boldsymbol{n}$ and $\boldsymbol{n}$ is the outward unit normal to the solid surface. On the solid wall, the wall distribution function is given by

$$g_{lw}^+ = (n_w/\pi T_w) R_l \exp\left[E_l\left(1 - T_w^{-1}\right)\right]\exp\left[-(1/T_w)(\boldsymbol{v} - \boldsymbol{u}_w)^2\right]$$

$$\text{if} \quad \boldsymbol{v}\cdot\boldsymbol{n} > 0 \quad (39a)$$

$$h_{lw}^+ = \tfrac{1}{2} T_w g_{lw}^+ \quad (39b)$$

The density of the molecules diffusing from the surface, n_w, is not known a priori and may be found by applying the condition of zero mass flux normal to the surface at the wall. One has

$$n_w = -2\left(\frac{\pi}{T_w}\right)^{\frac{1}{2}} \sum_l \int_{-\infty}^{\infty}\int_{-\infty}^{\infty} v_n^- g_l^-(x, y, t, v_x, v_y)\, dv_x\, dv_y \quad (40)$$

where $v_n^- = (v_n - |v_n|)/2$.

The inflow and outflow boundary conditions are treated using characteristics-based boundary conditions that are in accord with the upwind nature of the interior point scheme. For problems with symmetry, only half-plane is computed, and the symmetry condition is assigned to the distribution function.

In the slip flow regime, we also compare kinetic model solutions to Navier–Stokes solutions with slip boundary conditions. We use the following expressions for the slip velocity and temperature jump (in dimensionless form) at the wall for the Navier–Stokes model:

$$U_s = \frac{C_1}{\rho}\frac{M_\infty}{Re_\infty}\sqrt{\frac{2\gamma}{T_T}}\frac{\partial u_s}{\partial n} + \frac{2C_2}{\rho}\frac{M_\infty}{Re_\infty}\frac{1}{T_T}\frac{\partial T_T}{\partial s} \quad (41)$$

$$T_s - T_w = \frac{C_3}{2\rho}\frac{M_\infty}{Re_\infty}\frac{\gamma}{(\gamma - 1)Pr}\sqrt{\frac{\pi\gamma}{2T}}\frac{\partial T_T}{\partial n} \quad (42)$$

where U_s is the slip velocity, s and n denote the tangential and normal directions to the wall surface, $u_s = \boldsymbol{u}\cdot\boldsymbol{s}$, γ denotes the ratio of specific heats, and the Prandtl number $Pr = 0.72$; C_1, C_2, and C_3 are dimensionless constants depending on the molecular interaction model at the wall. Here, we follow Kogan[20] and take $C_1 = 1.012$, $C_2 = 0.383$, and $C_3 = 0.8155$. For all calculations in slip flow conditions, the thermal accommodation coefficient was set equal to unity (perfect accommodation). The slip velocity and the temperature jump are being calculated at each step of integration.

V. Results and Discussions

Several representative rarefied gas dynamical problems are computed in this section to illustrate the numerical methods as well as the statistical models for gases with and without internal degrees of freedom. Comparisons with corresponding results for monatomic gases and with experimental data are emphasized. Additional computational results using several Krook-type kinetic models for a monatomic gas and comparison with experimental results can be found in Ref. 11, where a different numerical method was used.

One-Dimensional Rarefied Riemann Shock-Tube Problem

The first example we considered is the one-dimensional unsteady Riemann shock-tube problem. The numerical treatment of this Riemann shock-tube problem has been studied by Chu[17] and recently by Prendergast and Xu[21] using the BGK kinetic model description. In this problem a diaphragm, which is located at $x = 0.5$, separates two regions, each in a constant equilibrium state at $t = 0$. For a monatomic gas, the initial conditions are $\rho = 10$, $T = 1.667$, and $u = 0.0$, for $0 \le x \le 0.5$, and $\rho = 1.0$, $T = 1.333$, and $u = 0$, for $0.5 < x \le 1$. For a diatomic gas, the initial conditions are $\rho = 10$, for $T = 1.4$, and $u = 0$, for $0 \le x \le 0.5$, and $\rho = 1.25$, $T = 1.12$, and $u = 0$, for $0.5 \le x \le 1$. The length of the tube is unity, which represents 1000 λ_R, where λ_R is the mean free path based on the right state. We used 100 grid points with physical spacing $\Delta x = 0.01$. In the velocity space, we used 20 discrete velocity points ranging from -5.3 to 5.3. The Gauss–Hermite quadrature formula was used. In the internal energy space, 10 discrete energy levels were used. The Courant number based on the maximum gas velocity, $|\lambda_i|_{\max}\Delta t/\Delta x$, is taken to be 0.9. The results of computed nondimensional flow properties at time $t = 0.1912$ are presented. At this moment, a shock wave is located near $x = 0.78$, a contact

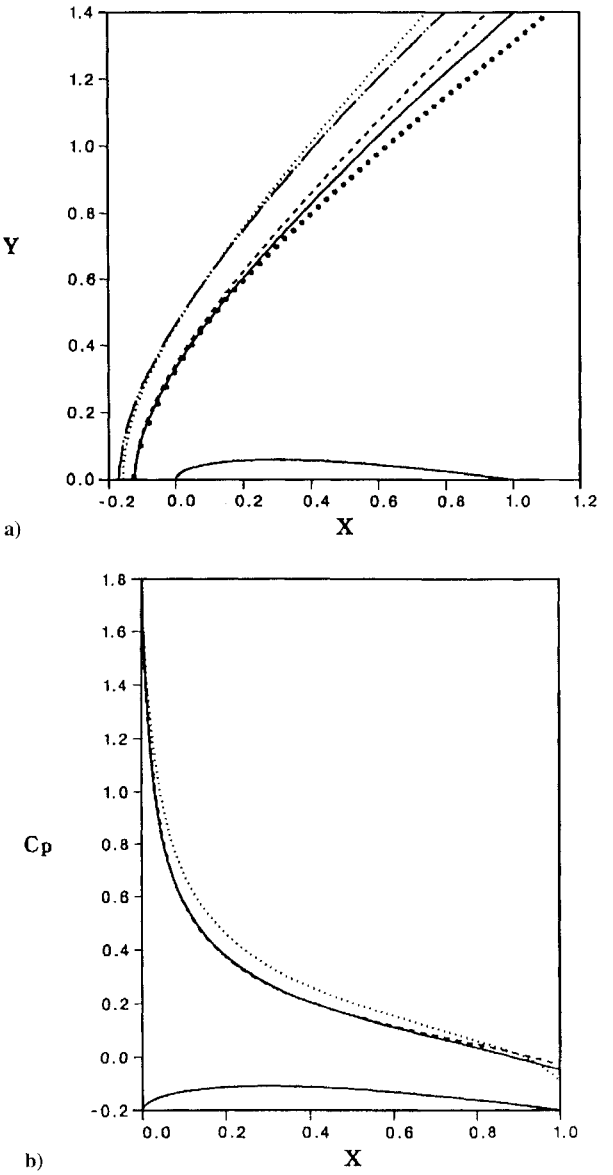

Fig. 7 Comparison of several physical models for supersonic flows past a NACA 0012 airfoil ($M_\infty = 2.0, Re_l = 1.06 \times 10^2, Kn_\infty = 0.03$, and $\alpha = 0$ deg). a) Shock shape and standoff distance and b) surface pressure coefficients: ····, Navier–Stokes; – – –, Navier–Stokes plus slip condition: —— diatomic model, – · –, monatomic model; and •, experiment (Allegre).

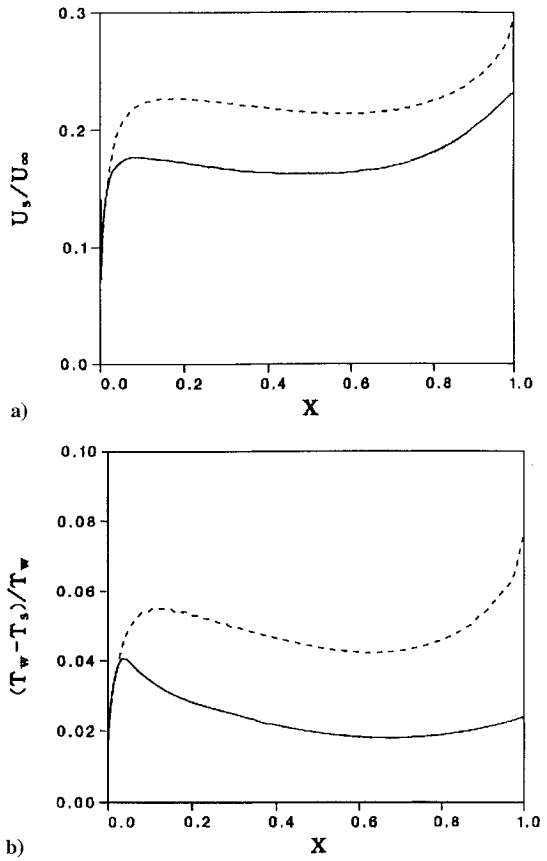

Fig. 8 Surface slip properties for supersonic rarefied flows past a NACA 0012 airfoil ($M_\infty = 2.0, Re_l = 1.06 \times 10^2, Kn_\infty = 0.03$, and $\alpha = 0$ deg). a) Slip velocity and b) temperature jump: ---, Navier–Stokes slip condition and ——, diatomic model.

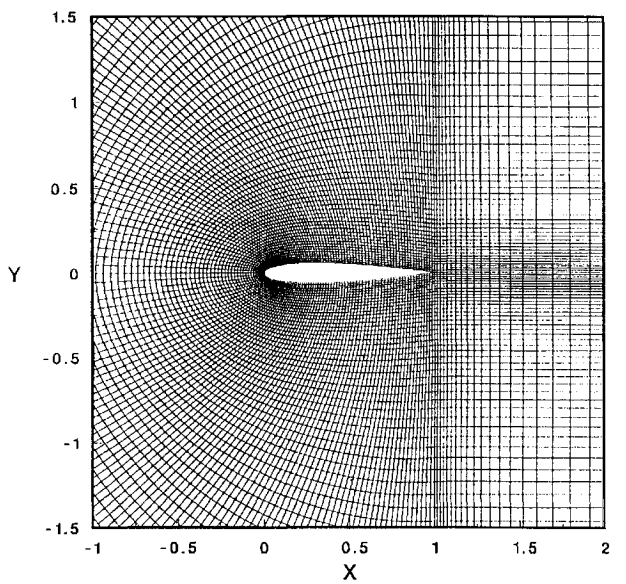

Fig. 9 C-type grid (201 × 51) system for NACA 0012 airfoil flow computation.

surface at $x = 0.65$, and an expansion fan at $x = 0.3$. The results (denoted as symbols) with $\Delta x = 10\lambda_R$ using ENO2 scheme for the BGK model are shown in Fig. 1. The results for the Morse–Holway model for diatomic gases are shown in Fig. 2. The solid lines that represent exact solutions of the Riemann problem of inviscid gas dynamics are shown for qualitative comparison. For the Euler exact solutions, the ratios of specific heats are chosen to be $\gamma = \frac{5}{3}$ and $\frac{7}{5}$ for monatomic and diatomic gases, respectively. The lower

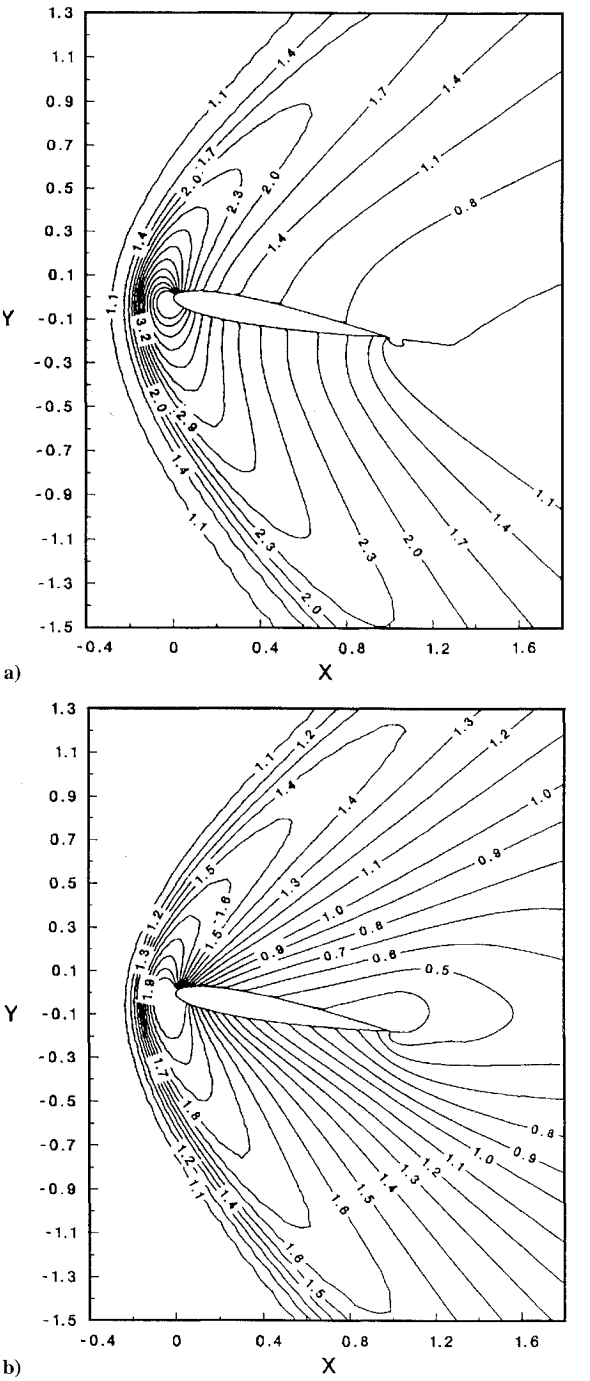

Fig. 10 Supersonic rarefied flow past a NACA 0012 airfoil ($M_\infty = 2.0, Re_l = 1.06 \times 10^2, Kn_\infty = 0.03$, and $\alpha = 10$ deg). BGK model for a monatomic gas: a) pressure contours and b) density contours.

total temperature for the diatomic gases can be explained by the fact that there exist other energy modes besides the translational energy. We also examine the effect of high-order schemes. In Fig. 3 the density and total temperature profiles for diatomic gases using first-order upwind, second-order TVD and second- and third-order ENO schemes are plotted. We can observe that high-order ENO schemes give crisper shock and contact profiles. A comparison of distributions of translational heat flux (i.e., q_t) along the tube for a monatomic gas (BGK model) and a diatomic gas (Morse–Holway model) is shown in Fig. 4. The CPU seconds needed per integration step for the ENO3 scheme are 0.026 and 0.237 s on a Cray Y-MP/EL computer for the BGK and Morse–Holway models, respectively.

Steady Rarefied Airflow Past a NACA 002 Airfoil

For two-dimensional steady problems, we considered a steady rarefied gas flow past a NACA 0012 airfoil. Experimental density

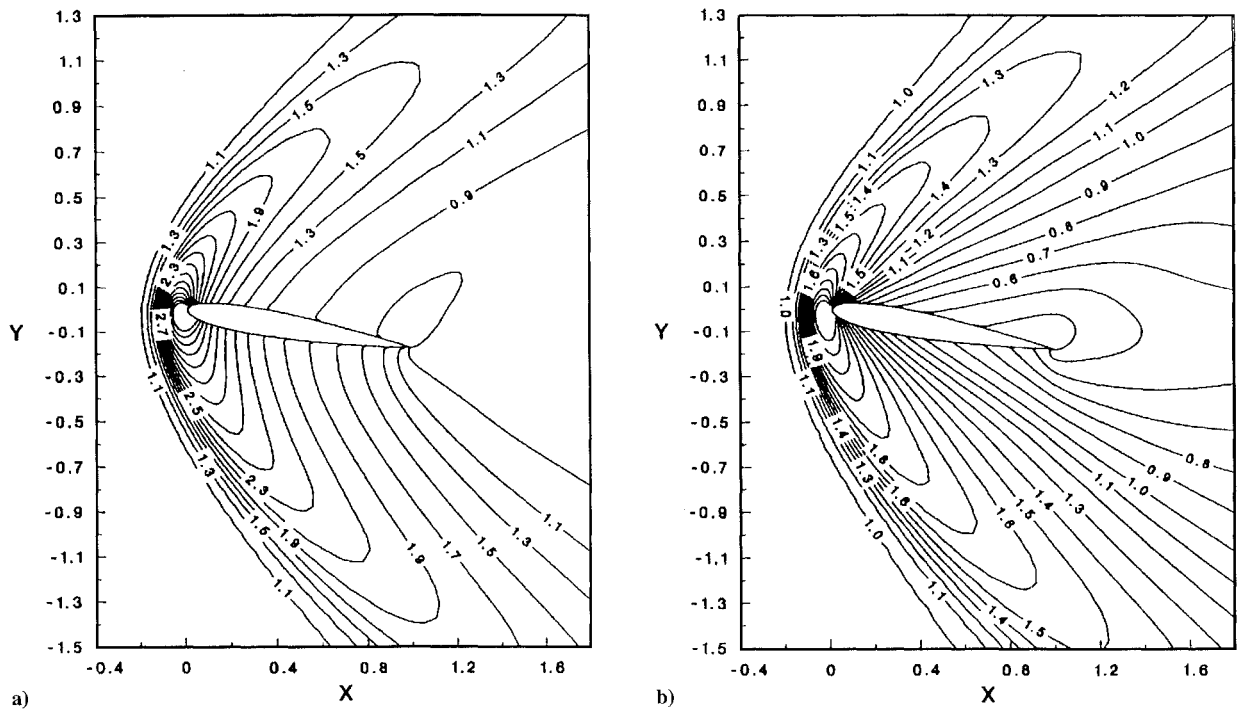

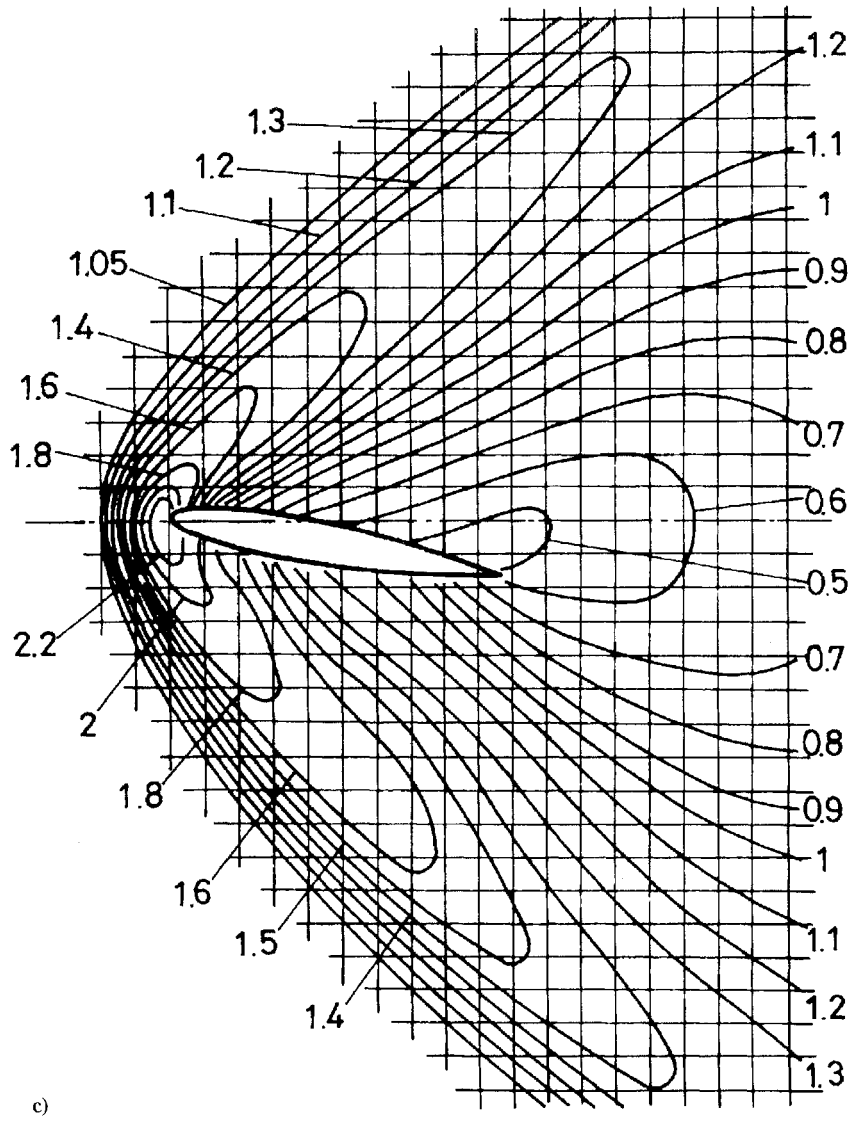

Fig. 11 Supersonic rarefied flow past a NACA 0012 airfoil ($M_\infty = 2.0, Re_l = 1.06 \times 10^2, Kn_\infty = 0.03$, and $\alpha = 10$ deg). Morse–Holway model for a diatomic gas: a) pressure contours, b) density contours, and c) experiment.[22]

flowfields around NACA 0012 airfoils for subsonic and supersonic cases under rarefied conditions have been obtained by Allegre et al.[22,23] We shall calculate their cases for 0- and 10-deg angles of attack and compare with their experimental results. We present the results for diatomic gases and compare them with those for monatomic gases and with experimental results. The steady-state solutions of rarefied gas flows are obtained using the LU implicit TVD method. Convergence of a steady-state solution is assumed to have occurred when L_2 norm of the residual is reduced to less than 10^{-4}. The wall temperature T_w of the airfoil is equal to the stagnation temperature of the flow and is about 290 K. The Reynolds number based on the airfoil chord length is about $Re_l = 1.06 \times 10^2$. A 101×71 C-type grid system was used. The number of discrete velocity points used in the (v_x, v_y) plane is (26×26), and the modified half-range Gauss–Hermite quadrature formula is used. For the diatomic gases, the number of discrete energy levels employed is 4, and the Gauss–Laguerre quadrature formula is used. The freestream Mach number is $M_\infty = 2.0$ and the Knudsen number $Kn_\infty = 0.03$. The computed results of pressure and density contours at 0-deg angle of attack are shown in Fig. 5 using the BGK model for a monatomic gas. In Fig. 6, the results of pressure, total temperature, and density contours at 0-deg angle of attack using the Morse–Holway model for a diatomic gas are shown together with the experimental density fields.

In general, both the Krook-type models for the monatomic and diatomic gases capture the flow structures including the bow shock and the stagnation region quite well. However, some discrepancy between BGK model results and the experimental data can be observed. The computed front bow shock in Fig. 5b is pushed farther away from the leading edge of the airfoil (i.e., larger shock standoff distance) as compared with experimental data, as shown in Fig. 6c. The results of the diatomic model are in good agreement with the experimental data. A comparison of the location and shape of front bow shock and surface pressure coefficients using several physical models is given in Fig. 7. The continuum Navier–Stokes model with no-slip and with slip boundary conditions, the BGK model for monatomic gases, and Morse–Holway model for diatomic gases are computed. The computed front bow shocks using both the BGK model and Navier–Stokes model with no-slip boundary conditions give larger shock standoff distances, $0.2L$ and $0.19L$, respectively. The Navier–Stokes model with slip boundary conditions gives a shock standoff distance around $0.16L$, and the Morse–Holway model gives a value of $0.15L$ that compares well with the experimental data. The Morse–Holway model produces the best results. The Navier–Stokes model with slip boundary conditions [Eqs. (41) and (42)] gives surprisingly good agreement with the diatomic gas model. Although we cannot find experimental data for comparison, however, we still display the velocity slip and temperature jump in Fig. 8 for the Navier–Stokes model with slip boundary conditions and the Morse–Holway model. Note that the numerical method used to solve the Navier–Stokes equations here is a high-order nonoscillatory LU implicit scheme similar to the present one with viscous terms discretized using second-order central differcing.

Finally, we consider the airfoil case with angles of attack. We report only the case for angle of attack $\alpha = 10$ deg, and the flow parameters are $M_\infty = 2.0$, $Kn_\infty = 0.03$, and $Re_l = 1.06 \times 10^2$. A 201×51 C-type grid system as shown in Fig. 9 was used. The pressure and density contours computed using the BGK model for a monatomic gas are shown in Fig. 10. The corresponding results using the Morse–Holway model for a diatomic gas are shown in Fig. 11, together with the experimental density fields.[22] By comparing the computed density contours from various kinetic models with the experimental data, it is quite evident that almost all of the major flow structures can be modeled well by the kinetic models chosen, and good flow resolution can be achieved with the present method. The results from the Morse–Holway model are closer to the experimental data. For a typical case run, it takes about 1000 iterations using a Courant number equal to 5 to reach a steady-state solution. That the smaller Courant number can be used (compared with 30 for monatomic gases) in diatomic gases may be attributed to the internal energy levels that make the problem more stiff.

VI. Conclusions

In this study, high-order nonoscillatory schemes for solving the nonlinear kinetic model equations for gases with and without internal degrees of freedom have been presented for the computations of rarefied gas flows. The BGK kinetic model for monatomic gases and the Morse–Holway model for gases with internal degrees of freedom are considered. In the method the discrete ordinate method for kinetic theory is first applied to the distribution function in phase space to remove its velocity dependence. The physical discrete internal energy states are assumed to be closely spaced and considered as a continuous energy space, and a Gauss–Laguerre quadrature is employed to rediscretize the energy space. This enables the resulting set of equations to be cast into conservation law form with source terms in physical space. Then the characteristic flux difference splitting method, in conjunction with the modified flux approach, is employed to produce a class of high-order ENO schemes for solving the kinetic model equations. For multidimensional problems, a general curvilinear coordinates system is used. The operator splitting is employed in the explicit method for unsteady flows, and the LU method was employed in the implicit methods for steady-state calculations. Computations of one- and two-dimensional rarefied gas flows indicate that both high resolution of flowfields and good qualitative agreement with theoretical and experimental results can be obtained. The present approach is quite general and applicable to rarefied gas flows over a wide range of Knudsen numbers. The only assumption is that the model equation instead of the full Boltzmann equation is used. Although the accuracy and applicability of the statistical models need further comparison with experimental results, the numerical methods developed in the present study for both monatomic gases and gases with internal degrees of freedom may serve as a useful tool to exploit many aspects of the kinetic models by exhibiting accurate results for many practical rarefied gas dynamical problems.

Acknowledgment

This work was sponsored by the National Science Council of the Republic of China under Grant NSC 84-0424-E002-001.

References

[1]Bird, G. A., *Molecular Gas Dynamics*, Oxford Univ. Press, London, 1976.

[2]Bird, G. A., *Molecular Gas Dynamics and Direct Simulation of Rarefied Gas Flows*, Oxford Univ. Press, London, 1994.

[3]Bhatnagar, P. L., Gross, E. P., and Krook, M., "A Model Collision Processes in Gases. I. Small Amplitude Processes in Charged and Neutral One-Component System," *Physical Review*, Vol. 94, No. 3, 1954, pp. 511–525.

[4]Morse, T. F., "Kinetic Model for Gases with Internal Degrees of Freedom," *Physics of Fluids*, Vol. 7, No. 2, 1964, pp. 159–169.

[5]Holway, L. H., Jr., "New Statistical Models for Kinetic Theory: Methods of Construction," *Physics of Fluids*, Vol. 9, No. 5, 1966, pp. 1658–1673.

[6]Chapman, S., and Cowling, T. G., *Mathematical Theory of Non-Uniform Gases*, 3rd ed., Cambridge Univ. Press, Cambridge, England, UK, 1990.

[7]Liepmann, H. W., Narashima, R., and Chahine, M. T., "Structure of a Plane Shock Layer," *Physics of Fluids*, Vol. 5, No. 8, 1962, pp. 1313–1324.

[8]Segal, B. M., and Ferziger, J. H., "Shock Wave Structure Using Nonlinear Model Boltzmann Equations," *Physics of Fluids*, Vol. 15, No. 7, 1972, pp. 1233–1247.

[9]Huang, A. B., and Hwang, P. F., "Test of Statistical Models for Gases With and Without Internal Energy States," *Physics of Fluids*, Vol. 16, No. 3, 1973, pp. 466–475.

[10]Huang, A. B., Hwang, P. F., Giddens, D. P., and Srinivasan, R., "High Speed Leading Edge Problem," *Physics of Fluids*, Vol. 16, No. 5, 1973, pp. 814–824.

[11]Yang, J. Y., and Huang, J. C., "Rarefied Flow Computations Using Nonlinear Model Boltzmann Equations," *Journal of Computational Physics*, Vol. 120, No. 2, 1995, pp. 323–339.

[12]Huang, A. B., and Giddens, D. P., "Discrete Ordinate Method for the Linearized Boundary Value Problems in Kinetic Theory of Gases," *5th International Symposium on Rarefied Gas Dynamics*, edited by C. L. Brundin, Academic, New York, 1967, pp. 481–505.

[13]Shizgal, B., "Gaussian Quadrature Procedure for Use in the Solution of Boltzmann Equation and Related Problems," *Journal of Computational Physics*, Vol. 41, No. 2, 1981, pp. 309–327.

[14]Yang, J. Y., "Third Order Nonoscillatory Schemes for the Euler Equations," *AIAA Journal*, Vol. 29, No. 10, 1991, pp. 1611–1618.

[15]Harten, A., "High Resolution Schemes for Hyperbolic Conservation Laws," *Journal of Computational Physics*, Vol. 49, No. 2, 1983, pp. 357–386.

[16]Harten, A., Engquist, B., Osher, S., and Chakravarthy, S., "Uniformly High-Order Accurate Nonoscillatory Schemes, III," *Journal of Computational Physics*, Vol. 71, No. 2, 1987, p. 231.

[17]Chu, C. K., "Kinetic-Theoretic Description of the Formation of a Shock Wave," *Physics of Fluids*, Vol. 8, No. 1, 1965, pp. 12–22.

[18]Jameson, A., and Yoon, S., "Lower-Upper Implicit Schemes with Multiple Grids for the Euler Equations," *AIAA Journal*, Vol. 26, No. 9, 1988, pp. 1025, 1026.

[19]Shih, T. I. P., and Chyu, W. J., "Approximate Factorization with Source Terms," *AIAA Journal*, Vol. 29, No. 10, 1991, pp. 1759, 1760.

[20]Kogan, M. N., "Molecular Gas Dynamics," *Annual Review of Fluid Mechanics*, Vol. 5, 1973, pp. 383–404.

[21]Prendergast, K. H., and Xu, K., "Numerical Hydrodynamics from Gas-Kinetic Theory," *Journal of Computational Physics*, Vol. 109, No. 1, 1993, pp. 53–66.

[22]Allegre, J., Raffin, M., and Lengrand, J. C., "Experimental Flowfields Around NACA 0012 Airfoils Located in Subsonic and Supersonic Rarefied Air Streams," *Proceedings of GAMM Workshop on Numerical Simulation of Compressible Navier–Stokes Flows* (Nice, Italy), Vieweg, Braunschweig, Germany, 1985, pp. 59–68.

[23]Allegre, J., Raffin, M., and Gottesdiener, L., "Slip Effect on Supersonic Flowfields Around NACA 0012 Airfoils," *Proceedings of the 15th International Symposium on Rarefied Gas Dynamics*, edited by V. Boffi and C. Cercignani, Teubner, Stuttgart, Germany, 1986, pp. 548–557.